Controlled Growth of High-Quality ZnO-Based Films and Fabrication of Visible-Blind and Solar-Blind Ultra-Violet Detectors

By *Xiaolong Du,* Zengxia Mei, Zhanglong Liu, Yang Guo, Tianchong Zhang, Yaonan Hou, Ze Zhang, Qikun Xue,* and *Andrej Yu Kuznetsov*

ZnO is a wide-bandgap (3.37 eV at room temperature) oxide semiconductor that is attractive for its great potential in short-wavelength optoelectronic devices, in which high quality films and heterostructures are essential for high performance. In this study, controlled growth of ZnO-based thin films and heterostructures by molecular beam epitaxy (MBE) is demonstrated on different substrates with emphasis on interface engineering. It is revealed that ultrathin AlN or MgO interfacial layers play a key role in establishing structural and chemical compatibility between ZnO and substrates. Furthermore, a quasi-homo buffer is introduced prior to growth of a wurtzite MgZnO epilayer to suppress the phase segregation of rock-salt MgO, achieving wide-range bandgap tuning from 3.3 to 4.55 eV. Finally, a visible-blind UV detector exploiting a double heterojunction of n-ZnO/insulator-MgO/p-Si and a solar-blind UV detector using MgZnO as an active layer are fabricated by using the growth techniques discussed here.

1. Introduction

ZnO is an attractive wide direct band gap (3.37 eV at room temperature) oxide semiconductor with a high exciton binding energy (60 meV), which makes it suitable for fabrication of short-wavelength optoelectronic devices, such as ultra-violet (UV) detectors, and UV and blue light emitting devices.[1] In the realization of all these applications, it is essential to prepare high-quality ZnO films and heterostructures. Despite the extensive research and the progress achieved in growing ZnO on various substrates, including both polar and non-polar ones, a microscopic characterization of the initial growth stages is still lacking. Such information is significant for realizing unipolar epitaxy because the initial stacking sequence of the Zn−O bilayer establishes the film's polarity and the subsequent growth can be considered homoepitaxy on this layer. In this news, controlled growth of ZnO-based thin films and heterostructures by molecular beam epitaxy (MBE) has been demonstrated on different substrates.

$Mg_xZn_{1-x}O$ films with tunable band gaps are promising active components in UV light emitters,[2] solar-blind UV detectors, as well as in other optoelectronic UV-range devices that rely on heterostructure functionalities.[3] Reproducible preparation of wurtzite MgZnO with high Mg content, however, is difficult to achieve due to phase segregation of rock-salt MgO. Therefore, it is significant to develop growth techniques that suppress phase segregation. In this part, we discuss the growth of single-phase wurtzite $Mg_xZn_{1-x}O$ alloys ($x = 0$ to 0.55) on sapphire substrate. By introducing a low Mg content MgZnO layer as a quasi-homo buffer for the epitaxy of high Mg content MgZnO, the phase segregation of rock-salt MgO is effectively suppressed. This bandgap engineering method proves very successful in the fabrication of solar-blind UV detectors.

Recently, both Schottky contact and p–n junction types of ZnO-based UV photodetectors have been realized and reported.[4] Because of the lack of stable and controllable p-type ZnO films, in most cases, heterojunctions were used to fabricate ZnO-based UV photodetectors with a different p-type semiconductor, such as Si.[5–7] However, while the n-ZnO/p-Si photodetectors that have been reported so far do have an increased UV photoresponse due to ZnO, they still have a notable photoresponse to visible light, which limits their direct application in UV detection in a visible light environment. In this study, a visible light-blind UV photodetector has been fabricated by exploiting a double heterojunction of n-ZnO/insulator-MgO/p-Si grown by molecular beam epitaxy. The key role of the middle insulating MgO layer as a barrier layer for a minority carrier transport has been demonstrated.

[*] Prof. X. L. Du, Dr. Z. X. Mei, Dr. Y. Guo, Z. L. Liu, T. C. Zhang, Y. N. Hou
Beijing National Laboratory for Condensed Matter Physics
Institute of Physics, Chinese Academy of Sciences
Beijing 100190 (P. R. China)
E-mail: xldu@aphy.iphy.ac.cn
Prof. Z. Zhang
Beijing University of Technology
Beijing 100022 (P. R. China)
Prof. Q. K. Xue
Department of Physics, Tsinghua University
Beijing 100084 (P. R. China)
Prof. A. Y. Kuznetsov
Department of Physics, University of Oslo
NO-0316 Oslo (Norway)

DOI: 10.1002/adma.200901108

2. Interface Engineering in ZnO Epitaxial Growth

The interface engineering usually begins with an appropriate pretreatment of the substrate to obtain the desired surface structure, on which a transition layer can be grown to bridge the structural and chemical differences. A ZnO buffer layer is then deposited at low temperature to relax misfit strain. One of our strategies is the use of ultra-thin AlN or MgO layers between the ZnO film and substrate to control the interface structure for unipolar ZnO films growth. The technique was successfully applied to ZnO epitaxy on sapphire,[8,9] spinel ($MgAl_2O_4$),[10] LSAT [$(La,Sr)(Al,Ta)O_3$],[11] etc. by radio frequency (RF)-plasma assisted molecular beam epitaxy (RF-MBE).

2.1. ZnO Epitaxy on Nitrided Sapphire Substrate

Due to the low cost, high crystal quality and stable chemical properties of sapphire substrate, it is the most favorable substrate currently used. However, the problem with sapphire is the formation of inversion domains (IDs), i.e., O-polar IDs in Zn-polar matrix, or Zn-polar IDs in an O-polar matrix. To solve the problem, surface nitridation was performed on sapphire substrate, and the influence of nitridation conditions on the formation of AlN/sapphire interfacial layers was systematically investigated. It was found that the nitridation temperature is crucial for achieving quality AlN buffer layers and ZnO films with cation or anion polarities, as demonstrated by *ex situ* transmission electron microscopy (TEM).

Our results show that both low temperature (LT) and high temperature (HT) nitridations under optimized nitrogen plasma conditions lead to the formation of a well-defined cubic phase of AlN. It is well established that the nitridation process begins with the bond formation between the nitrogen atoms and the first Al layer on the sapphire surface. The nitridation goes on with the diffusion of nitrogen atoms into sapphire and substitution for oxygen atoms, resulting in the formation of AlN thin layer. An Al-terminated surface is expected after HT thermal annealing under ultrahigh-vacuum conditions. For these topmost Al atoms, the coordination will be different from that in bulk. A tetrahedral environment, i.e., binding to three oxygen atoms in the layer below and leaving one dangling bond on the top, will be adopted rather than the octahedral one. When nitridation begins on this kind of surface at HT, the substitution of N atoms for the four coordinated underlying oxygen atoms will lead to the formation of an Al−N bilayer with the Al layer upward. Therefore, Al-polar AlN film will be formed as the diffusion of nitrogen atoms continues, which is demonstrated in the cross-sectional high-resolution TEM (HRTEM) image (Fig. 1a).

On the other hand, after sufficient exposure to oxygen radicals at LT, an oxygen-terminated surface of sapphire (0001) is expected. The underlying Al atoms are six coordinated, i.e., binding to three oxygen atoms in the topmost layer and another three in the second oxygen layer beneath, as in the bulk. When nitridation is performed on this kind of surface at LT, first, nitrogen atoms will replace the topmost oxygen atoms forming an AlNO complex that is unstable in terms of energy and will change into AlN when nitrogen substitution continues. In this way, a N−Al bilayer is formed with the N layer upward (i.e., the formation of N-polar AlN film). The thickness of AlN layer increases with the nitrogen substitution going on in the sapphire substrate and the structure of the N-polar AlN is extended; such is the case in Fig. 1b. Therefore, to ensure the uniformity of O-polar or Zn-polar ZnO films, the combination of sapphire surface pretreatment and nitridation temperature should be selected carefully so as to obtain a uniform coordination of the Al atoms in the first Al layer.

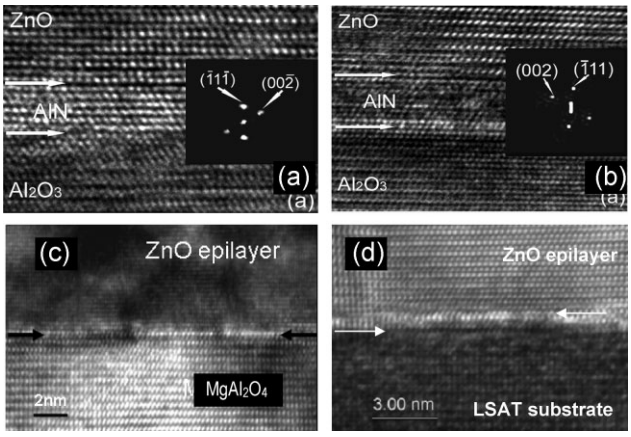

Figure 1. Cross-sectional HRTEM micrographs near the interface regions: a) Zn-polar ZnO/Al-polar AlN/sapphire interface, and, b) O-polar ZnO/N-polar AlN/sapphire interface, taken along the $[10\text{-}10]_{sapphire}$ direction (reproduced with permission from [7], copyright 2005 American Institute of Physics). c) ZnO/MgO/$MgAl_2O_4$ interface, taken along the $[10\text{-}10]_{ZnO}$ direction (reproduced with permission from [8], copyright 2007, American Institute of Physics). d) ZnO/MgO/LSAT interface, taken along the $[11\text{-}20]_{ZnO}$ direction (reproduced with permission from [9], copyright 2005, American Institute of Physics).

2.2. ZnO Epitaxy on Spinel ($MgAl_2O_4$) Substrate

High-quality GaN LD cavities could be obtained on $MgAl_2O_4$ (111) substrate simply by cleavage along the (−110) direction,[12] indicating that $MgAl_2O_4$ (111) is a promising substrate for fabricating ZnO LD cavities due to the similarities between ZnO and GaN. Previous experiments showed that when ZnO was directly grown on the above-mentioned surface, in many cases 30° rotation domains were formed due to the distortion of the oxygen sublattice. Control of the substrate surface structure is critical for reduction of rotation domains and inversion domains.

In our work, a magnesium wetting layer was used to modify the surface structure of the $MgAl_2O_4$ (111) substrate. By using Mg modification of an O-terminated $MgAl_2O_4$ (111) surface, we eliminated the 30° rotation domains and inversion domains and obtained high-quality ZnO films.

The substrates were first thermally cleaned at 780 °C and then pretreated by oxygen radicals at 130 °C. After Mg deposition in an ultrahigh vacuum at the same temperature, the substrate temperature was increased to 260 °C for about 10 min, and the same two step growth of ZnO was applied for growth of the films. It was found that this magnesium layer plays a crucial role in eliminating 30° rotation domains, reducing defect density, and

controlling the polarity of ZnO film, as demonstrated by in situ reflection high-energy electron diffraction (RHEED) and ex situ TEM.

Figure 1c shows a cross-sectional HRTEM image of the ZnO/MgO/$MgAl_2O_4$ interface region, taken along ZnO (10-10). It can be seen that the interface is atomically sharp without any amorphous layer or a layer with other structures. Hence, most of Mg atoms were re-evaporated and about 1 mL of Mg was left via the formation of Mg−O bond on the substrate surface, which is consistent with the fact that the RHEED patterns almost recover after the substrate temperature ramps to 260 °C (not shown here).

Obviously, the ultrathin MgO wetting layer plays a key role in the growth of single-domain O-polar ZnO film on $MgAl_2O_4$ (111) substrate. The O atoms and Mg atoms form a fcc-type structure with tetrahedral bonding, which influences the selection of the bond configuration of the MgO wetting layer. When the temperature increases to 260 °C, the Mg layer re-evaporates due to the high vapor pressure of $\sim 10^{-5}$ Torr; only one Mg layer, bound to the topmost oxygen atoms on the substrate surface, is left. The oxygen in the chamber will adsorb on this Mg layer, forming a uniform MgO wetting layer on the O-terminated $MgAl_2O_4$ (111) substrate. This MgO layer does not take its own structure but overlaps the oxygen sublattice of the substrate and inherits the tetrahedral bonding; i.e., each Mg atom forms a bond with the underlying O atom and three bonds with three oxygen atoms above. This tetrahedral bonded MgO wetting layer acts as a uniform template for the epitaxy of O-polar ZnO film.

2.3. ZnO Epitaxy on LSAT [(La,Sr)(Al,Ta)O_3] Substrate

(La,Sr)(Al,Ta)O_3(LSAT) is an excellent newly developed crystal that has already been used as substrate for high T_c superconductive film growth. LSAT (111) was once considered to be a promising substrate for GaN film, because theoretically, the lattice mismatch between GaN and LSAT (111) is less than 1%. However, experimental results showed that the actual crystallographic orientation for epitaxial GaN or AlN film on LSAT was rotated in-plane by 30° against the theoretical one, resulting in a much larger lattice mismatch than expected. A similar problem exists for ZnO epitaxy on LSAT (111). With the ideal in-plane alignment of $[11\text{-}20]_{ZnO}//[11\text{-}2]_{LSAT}$, the lattice mismatch between ZnO and LSAT is only ~2.9% compared to 18.9% for the $[10\text{-}10]_{ZnO}//[11\text{-}2]_{LSAT}$ alignment.

Hence, a ZnO/LSAT heterointerface is engineered to control the crystallographic orientation of ZnO films. Lattice-matched ZnO epitaxy (2.9%) with an in-plane alignment of $[11\text{-}20]_{ZnO}//[11\text{-}2]_{LSAT}$ has been realized on LSAT (111) by Mg modification of the substrate surface.

The substrates were preconditioned with oxygen radicals, and oxygen-terminated surfaces were expected after this pre-growth treatment. Mg was then deposited on this surface at 170 °C after the MBE chamber was vacuumized. The extra Mg was re-evaporated by annealing at 550 °C after an MgO layer was formed. Then, a conventional two-step growth of ZnO was performed; i.e., a low temperature buffer layer grown at 550 °C and a high temperature epilayer at 620 °C.

We found that this interface control technique – i.e., deposition and proper treatment of the Mg layer on the oxygen-terminated LSAT (111) – is essential for single-domain lattice-matched ZnO growth. The cross-sectional HRTEM image near the ZnO/MgO/LSAT interface (Fig. 1d) clearly shows that a continuous crystalline interface of 2 to 3 atomic layers was formed between ZnO and LSAT. The continuous crystalline feature of this interface layer suggests that a two-dimensional MgO wetting layer is formed, which is consistent with the streaky RHEED patterns (not shown here). The corresponding selected area diffraction pattern near the interface region verifies the lattice-matched crystallographic orientation of ZnO on LSAT (~3%).

3. Controlled Growth of MgZnO Films for Fabrication of Solar-Blind UV Detectors

Although much progress has been made in MgZnO technology recently, reproducible synthesis of solar-blind wurtzite MgZnO material remains a formidable challenge due to phase segregation of rock-salt MgO. Therefore, understanding and suppressing phase segregation plays a key role in high Mg-content alloy growth. In this part, a delicate control technique using an interfacial layer is developed for the growth of solar-blind wurtzite $Mg_{0.55}Zn_{0.45}O$ epilayer, in which a low Mg-content $Mg_{0.2}Zn_{0.8}O$ buffer layer is employed as a quasi-homoepitaxy template to accommodate the big difference in bonding configurations between Mg-O and Zn-O in a wurtzite structure. A photoconductive solar-blind UV detector is successfully fabricated, demonstrating the applicability of this bandgap engineering method.

The MgZnO samples were prepared on 2 inch sapphire (0001) wafers by RF-plasma assisted MBE. Elemental Mg (5 N) and Zn (7 N) evaporated by Knudsen cells (CreaTech) and radical oxygen generated by the RF-plasma system (SVTA) were used as sources for the growth. After loading into the chamber the substrates were heated up to 750 °C for thermal cleaning and subsequently exposed for oxygen plasma ''pre-treatment'' at 250 °C in order to obtain a uniform oxygen-terminated surface[13] on which synthesis of a quasi-homo MgZnO buffer (~20 nm) with a Mg content about 20% was performed. Finally, a high Mg-content MgZnO epilayer was grown on this template by increasing the Mg flux and keeping other growth conditions the same. In this way, the Mg-content in MgZnO epilayer can be controlled as long as the Mg flux is less than a critical value. For example, Sample A was prepared by using a Mg flux close to the critical value, while Sample B was prepared by using a Mg flux ~15% bigger, resulting in MgO phase segregation in this sample.

X-ray diffraction (XRD) θ–2θ scans were measured on all samples to study eventual phase segregation and Figure 2a illustrates the results obtained from Samples A and B. For Sample A, there are two peaks found, at 34.91° and 41.68°, corresponding to the W-MgZnO (002) and sapphire (006) planes, respectively. No other significantly strong signals related to other phases, suggesting that no phase segregation or emerging of RS-MgO occurs in the overgrown MgZnO film. A slight asymmetry in the W-MgZnO (002) peak can be explained by the contribution from the low Mg-content buffer underneath. Furthermore, the W-MgZnO (002) peak shifts to significantly larger angles

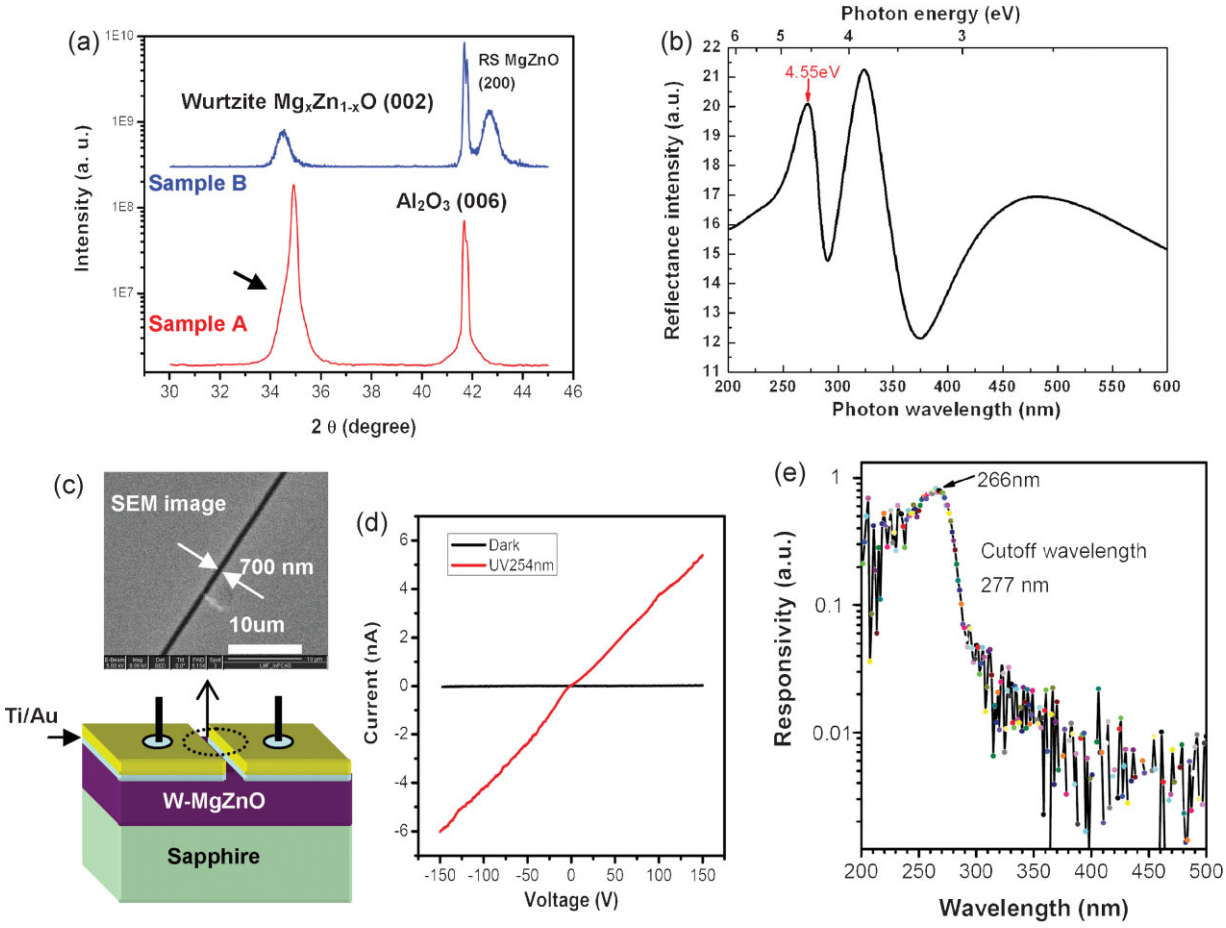

Figure 2. MgZnO film growth, properties and UV detector: a) XRD scans of MgZnO samples – no phase segregation is observed in Sample B. b) Reflectance spectrum taken from Sample A illustrating a bandgap of 4.55 eV, which is well within the solar-blind region. c) $Mg_{0.55}Zn_{0.45}O$ solar-blind UV detector structure where a narrow stripe (0.7 μm × 200 μm) etched by FIB technique serves as the active region. d) *I–V* characteristic of the photodetector, showing dark current and UV photocurrent at 254 nm. e) Response spectrum of a $Mg_{0.55}Zn_{0.45}O$ solar-blind photodetector at 150 V bias, demonstrating a sharp cut-off wavelength at 277 nm.

comparing to that for pure ZnO (002) – typically detected at ~34.46° – indicating that the *c* lattice parameter in the W-MgZnO decreases with increasing Mg content, relative to that of ZnO.[14] In its turn, the magnitude of the shift observed in Sample A implies an Mg fraction of 55% incorporated into the epilayer (also confirmed by Rutherford backscattering spectrometry, not shown here). Importantly, our synthesis of single phase W-MgZnO with a Mg content up to 55% is reproducible and controllable as long as the Mg flux is less than a critical value. In contrast, an extra peak at ~42.9° was observed in the XRD curve taken from Sample B (Fig. 2a) due to the existence of rock-salt MgO. On the other hand, this phase segregation occurs much more readily when the MgZnO epilayer is grown directly on sapphire substrate without a low Mg content buffer, in which case no wurtzite MgZnO film with an Mg fraction ≥45% could be obtained. Thus, our quasi-homo buffer approach extends the limits of Mg incorporation into W-MgZnO by at least 10%, leading to a breakthrough in reliable preparation of solar-blind MgZnO.

The bandgap of $Mg_{0.55}Zn_{0.45}O$ epilayer in Sample A was determined to be 4.55 eV according to the reflectance spectrum, as shown in Fig. 2b. A sharp peak at 4.55 eV, well within the solar-blind UV region, can be assigned to the film bandgap, which was also confirmed by the room temperature transmittance spectra taken from this sample (not shown here). To further demonstrate the optical properties of the alloy, a photoconductive UV detector was fabricated employing the wurtzite $Mg_{0.55}Zn_{0.45}O$ film by using a focused ion beam (FIB) technique, which is schematically shown in Fig. 2c. A 5 nm thick Ti was deposited by magnetron sputtering to serve as a contact layer with MgZnO, followed by deposition of an Au film (~35 nm) as a bonding pad. Then, a narrow stripe of the electrode with an area of 0.7 μm × 200 μm was completely etched by FIB, leaving the underlying MgZnO exposed to air. *I–V* characteristic measurements show that the MgZnO film is a semi-insulator with a dark current of 25 pA at 150 V bias (Fig. 2d). The photoresponse spectrum was measured under a bias of 150 V, as shown in Fig. 2e. A sharp cut off of responsivity can be seen at a wavelength of 277 nm, which corresponds to the near band edge absorption of MgZnO. The responsivity peak is at 266 nm, which demonstrates that the device can work well in the UV region in an environment of solar radiation, while greatly suppressing any response to the sun.

4. Preparation of ZnO/MgO/p-Si Heterostructures and Fabrication of Visible Light-Blind UV Detectors

The merit of wide band-gap semiconductor UV photodetectors is the large UV/visible rejection ratio in comparison with the narrow band-gap semiconductor UV photodetectors, such as Si ($E_g = 1.12$ eV), which exhibits a wide photoresponse spectrum covering the UV and visible region.

In our work, a novel design of a double heterojunction employs RF-MBE, and an n-ZnO/insulator-MgO/p-Si visible-blind ultraviolet (UV) photodetector was realized. Moreover, the key role of MgO in the suppression of visible light photoresponse in our device was demonstrated. The photoresponse spectrum indicates a visible-blind UV detectivity of our devices with a sharp cutoff of responsivity at a wavelength of 378 nm, which corresponds to the near band edge absorption of ZnO. Moreover, an obvious suppression of photoresponse to visible light can be observed.

To further indicate the effect of the middle i-MgO layer in our device, an n-ZnO/MgO(~6 nm)/p-Si double heterojunction was prepared and its photoresponse characteristic was compared with that of the n-ZnO/insulator-MgO(~50 nm)/p-Si heterojunction. Both dark current and photocurrent increase a lot as the thickness of the i-MgO layer decreases in the p–insulator–n heterojunction, resulting in a lower UV/visible rejection ratio. Therefore, it is necessary to form an MgO layer with good insulation, which can effectively prevent the electron injection from the p-Si side to the n-ZnO side at a reverse bias in both cases of dark and visible light illumination due to the high potential barrier of the MgO layer for electrons.

The MBE growth of a high-quality single crystalline ZnO (0001) film on Si (111) substrates by using a low-temperature interface engineering technique was reported in our previous study.[15] There, a thin MgO (111) layer was sandwiched between the Si (111) substrate and the top ZnO (0001) film to prevent the Si surface from oxidizing and to serve as nuclei for single-domain epitaxy of ZnO. A well-defined MgO layer below ZnO and an amorphous layer above Si can be clearly seen from the cross-sectional HRTEM image near the interface region (see Fig. 3a), suggesting that the good crystal quality of MgO is maintained during the temperature ramping and even after high-temperature growth of the ZnO epilayer, although severe degradation of the Mg(0001)/Si(111) interface occurs.

Then, the middle MgO layer was increased to 50 nm to form a double heterojunction of n-ZnO/insulator-MgO/p-Si (p–insulator–n), which retained the in-plane epitaxial relationship $[1010]_{ZnO}//[112]_{MgO}//[112]_{Si}$. Our UV photodetector fabricated based on this p–insulator–n double heterojunction contains a top ZnO (0001) layer which is an unintentionally doped n-type film with an electron concentration of $\sim 10^{16}$ cm^{-3} and a thickness of 500 nm while the Si substrate is a 2 inch commercial boron-doped p-type Si (111) wafer with a hole concentration of $\sim 10^{18}$ cm^{-3}. The ohmic contact on ZnO film is a circular Ti (~20 nm)/Au (~40 nm) electrode with a diameter of 300 μm, which was defined by the standard lithography technique and was deposited by magnetron sputtering, followed by annealing at 300 °C in a vacuum for 5 min. Indium was pasted on the back side of the p-Si wafer with a large area of ~1 mm^2 to serve as the ohmic electrode on p-Si.

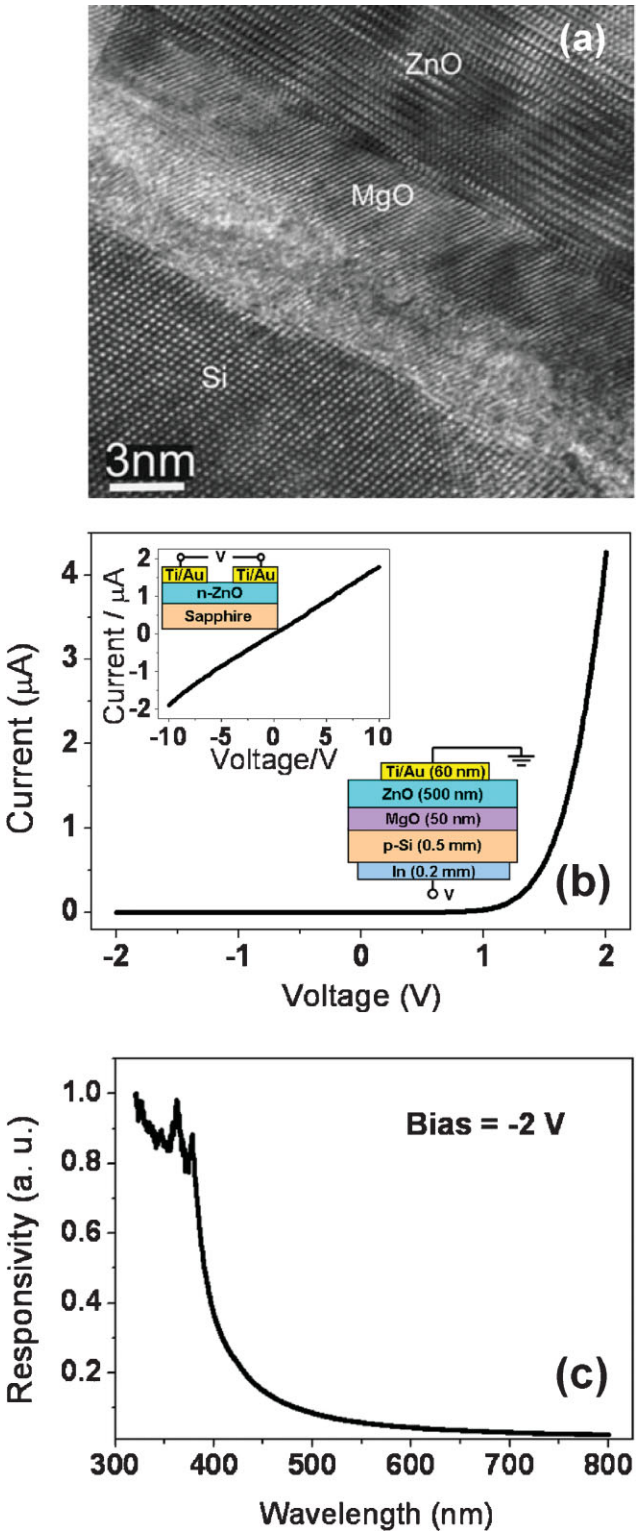

Figure 3. a) Cross-sectional HRTEM images along the $[10\text{-}1]_{Si}$ direction near the interface region (reproduced with permission from [10], copyright 2007, American Institute of Physics). b) the *I–V* characteristics of the photodetector based on n-ZnO/insulator-MgO/p-Si double heterojunction. c) Spectral responsivity of the n-ZnO/i-MgO/p-Si heterojunction photodetector at a reverse bias of −2 V (reproduced with permission from [16], copyright 2009, American Institute of Physics).

Figure 3b shows the current-voltage (*I–V*) characteristic of the p–insulator–n photodetector in dark. The ohmic contact of Au/Ti/ZnO is confirmed by the linear *I–V* curve in the inset of Figure 3b. The p–insulator–n photodetector in dark presents a typical rectifying characteristic of a p–n junction diode with a rectification ratio of $\sim 10^4$ at ± 2 V. Moreover, the reverse dark current is lower than 1 nA at -2 V.

The typical spectral responsivity of the p–insulator–n photodetector at a reverse bias of -2 V is shown in Figure 3c. A sharp cut off of responsivity can be seen at a wavelength of 378 nm, which corresponds to the near band edge absorption of ZnO, whereas almost no photoresponse was observed over the whole visible region. The UV/visible rejection ratio is about 45, which demonstrates that the device can work well in the UV region without the influence of visible light as a background.[16]

5. Conclusions and Perspectives

In this work, controlled growth of ZnO-based thin films by RF-MBE has been intensively studied with emphasis on interface and bandgap engineering. A three-step technique was developed and proved effective for high-quality ZnO film growth on different substrates, including: i) an appropriate substrate pretreatment to obtain desired surface structure, ii) interfacial layer design and preparation to establish structural and chemical compatibility between the layers, and iii) ZnO buffer layer deposition at low temperature to relax misfit strain.

We also demonstrated that the interfacial layer plays a key role in suppressing phase segregation in the MgZnO layer. A single-phase wurtzite $Mg_{0.55}Zn_{0.45}O$ thin film with a bandgap of 4.55 eV was successfully synthesized on quasi-homo $Mg_{0.2}Zn_{0.8}O$ buffers by RF-plasma assisted MBE, and it was demonstrated to be a suitable component for fabricating solar-blind UV detectors.

By using the low temperature interface engineering technique, a double heterojunction of n-ZnO/insulator-MgO/p-Si was prepared with a sharp interface between ZnO and MgO. This double heterojunction was then used to fabricate a visible-blind ultraviolet photodetector. A cut off of UV detectivity at a wavelength of 378 nm was observed, which indicates the photodetector has a photoresponse to ultraviolet but a rejection of visible light.

Acknowledgements

The Microfabrication lab in IPCAS is acknowledged for technical support during device fabrication. This work was supported by the National Science Foundation (grant nos. 50532090, 60606023, 60621091, 10804126) and the Ministry of Science and Technology (grant nos. 2007CB936203, 2009CB929400, 2009CB623700) of China, as well as by the Research Council of Norway through the FRINAT "Understanding ZnO" project. This article is part of a Special Issue on research at the Institute of Physics, Chinese Academy of Sciences.

Published online: September 15, 2009

[1] D. M. Bagnall, Y. F. Chen, Z. Zhu, T. Yao, M. Y. Shen, T. Goto, *Appl. Phys. Lett.* **1998**, *73*, 1038.
[2] A. Ohtomo, M. Kawasaki, I. Ohkubo, H. Koinuma, T. Yasuda, Y. Segawa, *Appl. Phys. Lett.* **1999**, *75*, 980.
[3] A. Tsukazaki, A. Ohtomo, T. Kita, Y. Ohno, H. Ohno, M. Kawasaki, *Science* **2007**, *315*, 1388.
[4] S. Liang, H. Sheng, Y. Liu, Z. Huo, Y. Lu, H. Shen, *J. Cryst. Growth* **2001**, *225*, 110.
[5] I.-S. Jeong, J. H. Kim, S. Im, *Appl. Phys. Lett.* **2003**, *83*, 2946.
[6] S. Mridha, D. Basak, *J. Appl. Phys.* **2007**, *101*, 083102.
[7] C. H. Park, K. S. Jeong, J. H. Kim, Seongil. Im, *Appl. Phys. Lett.* **2003**, *82*, 3973.
[8] Z. X. Mei, X. L. Du, Y. Wang, Z. Q. Zeng, H. Zheng, J. F. Jia, Q. K. Xue, Z. Zhang, *Appl. Phys. Lett.* **2005**, *86*, 112111.
[9] Y. Wang, X. L. Du, Z. X. Mei, Z. Q. Zeng, M. J. Ying, H. T. Yuan, J. F. Jia, Q. K. Xue, Z. Zhang, *Appl. Phys. Lett.* **2005**, *87*, 051901.
[10] Z. Q. Zeng, Y. Z. Liu, X. L. Du, H. T. Yuan, Z. X. Mei, J. F. Jia, Q. K. Xue, Z. Zhang, *Appl. Phys. Lett.* **2007**, *90*, 081911.
[11] M. J. Ying, X. L. Du, Y. Z. Liu, Z. T. Zhou, Z. Q. Zeng, Z. X. Mei, J. F. Jia, H. Chen, Q. K. Xue, Z. Zhang, *Appl. Phys. Lett.* **2005**, *87*, 202107.
[12] J. W. Yang, Q. Chen, C. J. Sun, B. Lim, M. Zubair Anwar, M. Asif Khan, H. Temkin, *Appl. Phys. Lett.* **1996**, *69*, 369.
[13] Z. X. Mei, Y. Wang, X. L. Du, M. J. Ying, Z. Q. Zeng, H. Zheng, J. F. Jia, Q. K. Xue, Z. Zhang, *J. Appl. Phys.* **2004**, *96*, 7108.
[14] A. Ohtomo, M. Kawasaki, T. Koida, K. Masubuchi, H. Koinuma, Y. Sakurai, Y. Yoshida, T. Yasuda, Y. Segawa, *Appl. Phys. Lett.* **1998**, *72*, 2466.
[15] X. N. Wang, Y. Wang, Z. X. Mei, J. Dong, Z. Q. Zeng, H. T. Yuan, T. C. Zhang, X. L. Du, J. F. Jia, Q. K. Xue, X. N. Zhang, Z. Zhang, Z. F. Li, W. Lu, *Appl. Phys. Lett.* **2007**, *90*, 151912.
[16] T. C. Zhang, Y. Guo, Z. X. Mei, C. Z. Gu, X. L. Du, *Appl. Phys. Lett.* **2009**, *94*, 113508.